PILS6 is a temperature-sensitive regulator of nuclear auxin input and organ growth in *Arabidopsis thaliana*

Elena Feraru[a,1], Mugurel I. Feraru[a], Elke Barbez[a], Sascha Waidmann[a], Lin Sun[a], Angelika Gaidora[a], and Jürgen Kleine-Vehn[a,1]

[a]Department of Applied Genetics and Cell Biology, University of Natural Resources and Life Sciences, 1190 Vienna, Austria

Edited by Zhenbiao Yang, University of California, Riverside, CA, and accepted by Editorial Board Member Natasha V. Raikhel January 16, 2019 (received for review August 14, 2018)

Temperature modulates growth and development throughout the entire lifecycle of a plant. High temperature (HT) triggers the auxin biosynthesis-dependent growth in aerial tissues. On the other hand, the contribution of auxin to HT-induced root growth is currently under debate. Here we show that the putative intracellular auxin carrier PIN-LIKES 6 (PILS6) is a negative regulator of organ growth and that its abundance is highly sensitive to HT. PILS6 localizes to the endoplasmic reticulum and limits the nuclear availability of auxin, consequently reducing the auxin signaling output. HT represses the PILS6 protein abundance, which impacts on PILS6-dependent auxin signaling in roots and root expansion. Accordingly, we hypothesize that PILS6 is part of an alternative mechanism linking HT to auxin responses in roots.

high temperature | auxin signaling | PILS proteins | endoplasmic reticulum | root growth

An increase in ambient temperature has dramatic consequences for plant development and threatens crop productivity. *Arabidopsis thaliana* is a suitable model system to investigate adaptation to temperature, displaying optimal growth at 22–23 °C (1). Temperatures above 27 °C are defined as high temperature (HT; 27–30 °C) or extremely HT (37–42 °C) (2) and severely affect various aspects of plant growth and development.

Phytohormones are important regulators to integrate external signals into the growth program, allowing for adaptive plant growth and development. The endogenous auxin indole-3-acetic acid (IAA) is a major plant growth regulator (3), which is also fundamentally important for adaptive responses to deviation in ambient temperature (4, 5). In aerial organs, such as hypocotyls and petioles, phytochrome B (phyB) functions as a thermoreceptor (6, 7). HT inactivates phyB, which derepresses the bHLH transcription factor phytochrome interacting factor 4 (PIF4), being crucial for aerial tissues to respond to HT (6, 7). Mechanistically, HT-induced PIF4 elevates auxin biosynthetic genes, which will consequently induce growth in aerial tissues (8–11).

Compared with the shoot, it remains mechanistically puzzling how elevated temperature impacts on root growth and development. An increase in temperature (26 °C–29 °C) also stimulates primary root growth in *Arabidopsis* seedlings (12–14). However, the underlying hormone-based mechanism is currently under debate. While several studies suggest that HT also affects root growth in an auxin-dependent manner (12, 13, 15), a recent study shows that brassinosteroid, but not auxin signaling, regulates warm temperature adaptation in roots (14). A central argument in the latter study is that, besides their prominent roles in shoots, PIF4 and its downstream auxin biosynthetic genes do not link temperature sensing with growth responses in roots (14).

The PIN-LIKES (PILS) proteins are putative auxin carriers at the endoplasmic reticulum (ER), where they stimulate intracellular auxin accumulation (16). PILS proteins, such as PILS2, PILS3, and PILS5, limit auxin signaling, likely by sequestering auxin in the ER (16–18). Notably, the importance of PILS2, -3, and -5 for light-induced growth in apical hook development was recently shown (18), proposing that PILS proteins integrate environmental signals to induce auxin signaling minima. Here we show that PILS6 is a temperature-sensitive regulator of nuclear availability of auxin, contributing to the increase of nuclear auxin signaling and root growth.

Results and Discussion

Relatively little is known about intracellular compartmentalization of auxin and the importance of the PILS intracellular auxin carrier family. We focused our attention on PILS6, because it is evolutionarily most distantly related to the so-far characterized PILS2, -3, and -5 proteins (18, 19). To assess the importance of PILS6 for seedling development, we isolated *pils6* full knockout mutants in *A. thaliana* (20) (*SI Appendix*, Fig. S1 *A* and *B*). Under standard growth conditions at 21 °C, the mutations in *pils6-1* and *pils6-2* induced overall increased organ growth, displaying longer primary roots, enlarged cotyledon area, as well as bigger rosette leaves (Fig. 1 *A*–*C*). To assess how constitutive PILS6 expression affects plant growth, we expressed a functional PILS6-GFP under the control of 35S promoter ($PILS6^{OE}$) and generated several independent, stable transgenic lines (*SI Appendix*, Fig. S2*A*). Conversely to *pils6* mutants, $PILS6^{OE}$ inhibited primary root growth and led to smaller cotyledons as well as rosettes (Fig. 1 *A*–*C*). The impact of PILS6 on root and rosette size is at least partly related to the regulation of cell division, because the *pils6* mutants and $PILS6^{OE}$ displayed stronger and weaker activity of the B1-type cyclin cell cycle marker (*CYCB1;1::GUS*) (21),

Significance

High temperature (HT) strongly modulates plant growth and eventually threatens yield stability. HT induces biosynthesis of the phytohormone auxin, which in turn increases cellular auxin levels and growth rates in shoots. This mechanism does not control HT-induced root growth and, hence, the role of auxin in this process is currently controversial. Here we show that the putative auxin carrier PIN-LIKES 6 (PILS6) localizes to the endoplasmic reticulum, where it gates nuclear auxin accumulation and perception. HT decreases the abundance of PILS6 proteins, consequently increasing nuclear auxin signaling and root growth. Our data dismantle current controversy, revealing an alternative subcellular mechanism in roots, which links PILS6-dependent control of cellular auxin sensitivity with HT-induced organ growth.

Author contributions: E.F., M.I.F., and J.K.-V. designed research; E.F., M.I.F., E.B., S.W., L.S., and A.G. performed research; E.F., M.I.F., E.B., S.W., and J.K.-V. analyzed data; and E.F. and J.K.-V. wrote the paper.

The authors declare no conflict of interest.

This article is a PNAS Direct Submission. Z.Y. is a guest editor invited by the Editorial Board.

[1]To whom correspondence may be addressed. Email: elena.feraru@boku.ac.at or juergen.kleine-vehn@boku.ac.at.

This article contains supporting information online at www.pnas.org/lookup/suppl/doi:10.1073/pnas.1814015116/-/DCSupplemental.

Published online February 12, 2019.

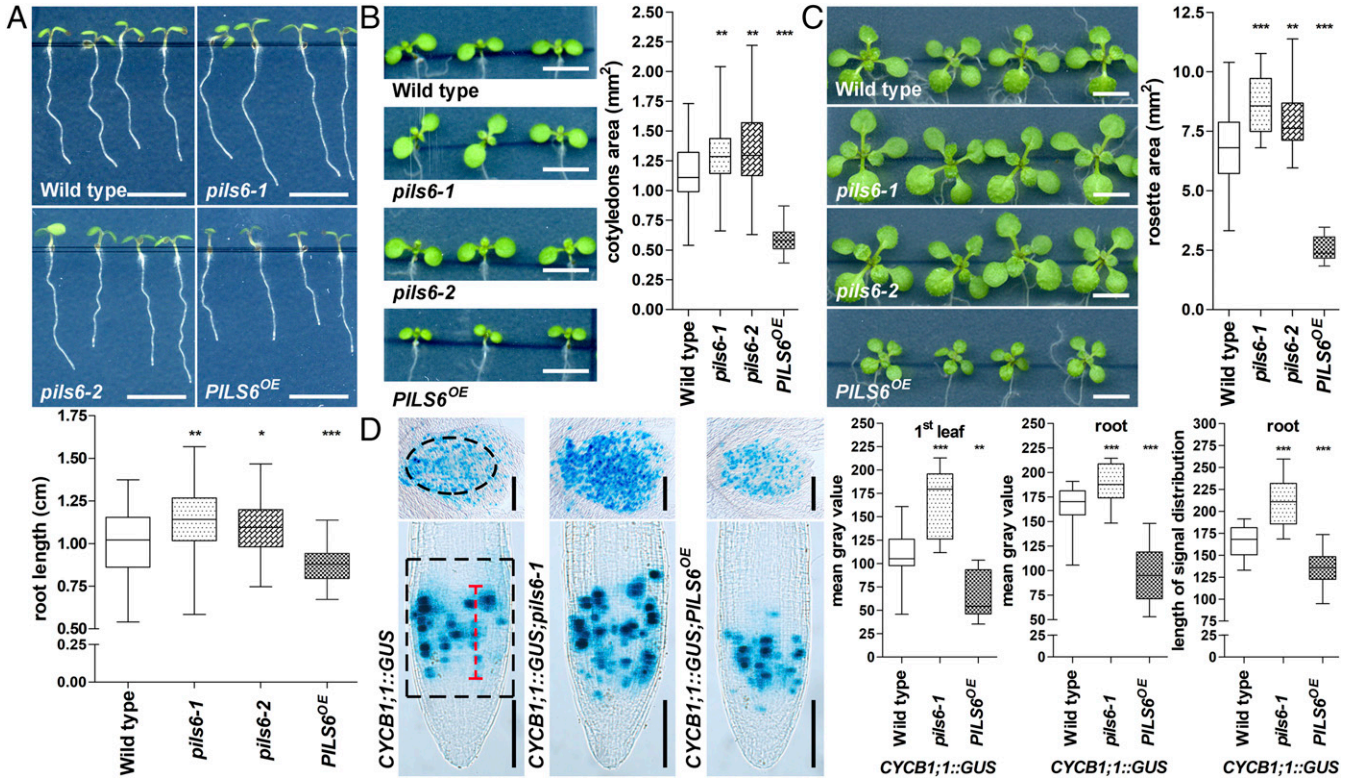

Fig. 1. PILS6 is a negative regulator of organ growth. (*A–C*) PILS6 affects organ growth. Scanned images and measurements show that total root length (*A*), cotyledon area (*B*), and rosette area (*C*) are affected in the *pils6* mutants and *PILS6*^{OE} compared with the wild-type control. (*D*) PILS6 affects cell division. GUS images and measurements of *CYCB1;1::GUS* expression (first leaf in *Upper* images, root in *Lower* images) and root meristem distribution show that cell division is affected in the *pils6* mutant and *PILS6*^{OE} compared with the wild-type control. The black dashed boxes represent the ROIs used to quantify *CYCB1;1::GUS* signal intensity. The red dashed line shows how the length of *CYCB1;1::GUS* distribution in the meristem was quantified. [Scale bars, 500 μm (*A–C*) and 100 μm (*D*).] n = 49–55 roots (*A*), 50–56 cotyledons (*B*), 28 rosettes (*C*), 10–12 first leaves (*D*), and 28 roots (*D*). *P = 0.01–0.05, **P = 0.001–0.01, ***P < 0.001, one-way ANOVA.

respectively (Fig. 1*D*). Also the expression domain (length) of *CYCB1;1::GUS* in roots was altered, suggesting longer and shorter root meristems in *pils6-1* and *PILS6*^{OE}, respectively (Fig. 1*D*). Altogether, these data indicate that PILS6 is a negative regulator of organ growth in *Arabidopsis*.

Next, we addressed the subcellular localization of PILS6-GFP in roots. Similar to functional PILS3-GFP (18) and PILS5-GFP (16), transgenic PILS6-GFP resided in perinuclear and reticular membranes, indicating localization at the ER in *Arabidopsis* roots and cotyledons (Fig. 2*A* and *SI Appendix*, Fig. S2 *A–C*). We also obtained a typical, albeit weaker, PILS6-GFP localization at the ER in roots when expressed under its endogenous promoter (Fig. 2*B* and *SI Appendix*, Fig. S2*D*). Notably, *pPILS6:PILS6-GFP* complemented the *pils6-1* mutant phenotype (*SI Appendix*, Fig. S2*E*), indicating that the ER-localized PILS6 proteins impact on organ size regulation.

PILS proteins have a presumed role in limiting auxin diffusion into the nucleus, due to an auxin compartmentalization mechanism at the ER (16–18, 22). We tested this assumption for PILS6 by using the nuclear auxin input reporters DII-VENUS (23) and its related ratio-metric version R2D2 (24). Nuclear DII/D2 domain displays auxin-sensitive degradation and, hence, the fluorescence of DII/D2-VENUS correlates inversely with the nuclear levels of auxin (23, 24), which allows us to indirectly monitor the nuclear availability of auxin. *pils6-1* mutant displayed remarkably reduced D2 fluorescence (Fig. 2*C* and *SI Appendix*, Fig. S2*G*), indicating substantially higher nuclear auxin levels in cells of the root apical meristem. We next assessed PILS6-dependent nuclear auxin signaling rates by using the auxin responsive promoter DR5 transcriptionally fused to GFP (*pDR5rev::GFP*) (25). In agreement with higher auxin accumulation in the nucleus, *pils6-1* mutant displayed increased nuclear auxin signaling in root tips (Fig. 2*D*).

On the other hand, *PILS6* overexpression enhanced nuclear DII-VENUS signal intensities in the root apical meristem (Fig. 2*E*) compared with the control and auxin insensitive mDII-VENUS line (Fig. 2*E* and *SI Appendix*, Fig. S2*F*). The reduced nuclear availability of auxin also correlated with diminished *pDR5rev::mRFP1er* (26) in *PILS6*^{OE}-expressing roots (Fig. 2*F*). Altogether, we conclude that PILS6 proteins limit nuclear levels of auxin and, similarly to PILS2, -3, and -5 proteins (16, 18), also negatively impact on nuclear auxin signaling output. Notably, *pils6* mutants displayed a very strong impact on the nuclear availability of auxin (as revealed by D2 and R2D2 markers), but a comparably weaker alteration in DR5-based auxin signaling rates. This observation may imply that additional processes (at the level of auxin perception or signaling output) modulate the nuclear auxin signaling output to partially compensate for the loss of *PILS6*.

We have recently revealed that phyB-dependent light perception induces *PILS2* and *PILS3* expression and thereby impacts on auxin-dependent growth regulation in apical hooks (18). These findings propose that *PILS* genes are developmentally important integrators of environmental cues. To further investigate the developmental role of PILS6, we, accordingly, looked for abiotic factors that may impact on *PILS6* expression. The evaluation of publicly accessible transcriptome data suggested that *PILS6* is particularly responsive to HT stress (27)

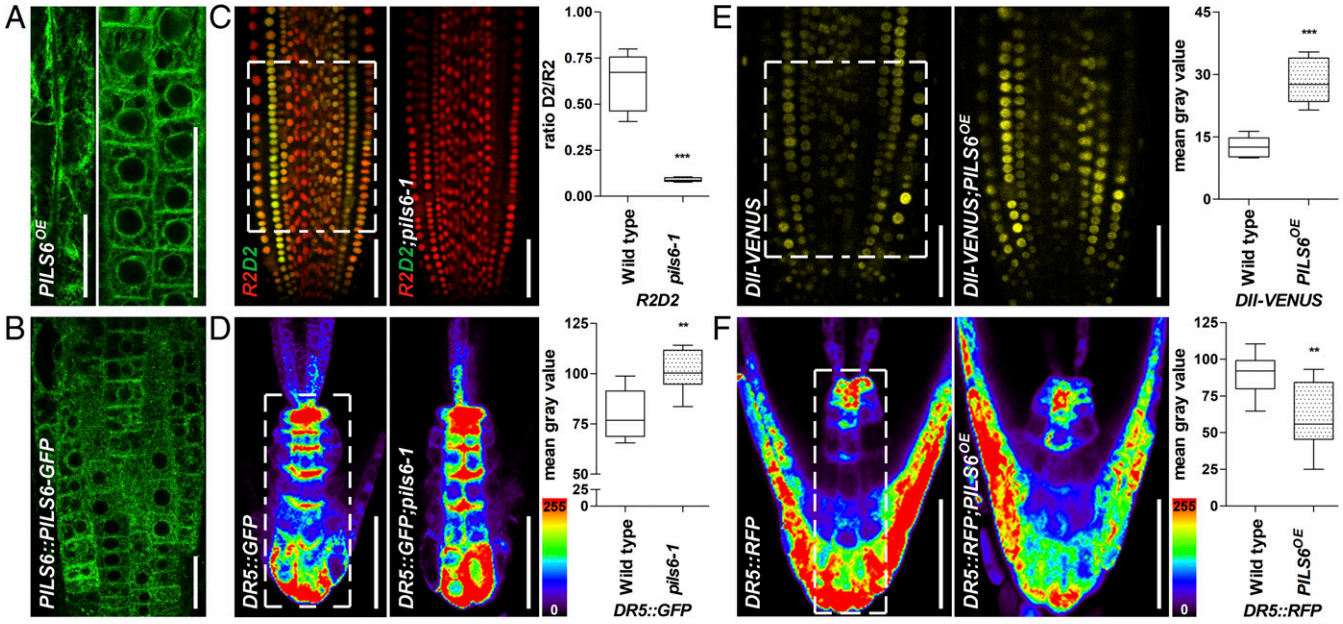

Fig. 2. ER-localized PILS6 affects the nuclear availability of auxin. (*A* and *B*) PILS6 localizes to the ER. Confocal images of PILS6-GFP in the elongated (*Left* image) and meristematic (*Right* image) cells of *PILS6*^{OE} (*A*) and meristematic cells of *PILS6::PILS6-GFP* (*B*) show ER-like distribution in roots. (*C*–*F*) PILS6 affects auxin signaling. Merged confocal images of R2 (red) and D2 (green) expressing R2D2 marker and quantification of D2/R2 ratio (*C*) show enhanced degradation of D2 signal in the *pils6-1* mutant. Pseudocolored confocal images and fluorescence intensity quantification of *DR5rev::GFP* (*D*) or *DR5rev::mRFP1er* (*F*) in the root tip show stronger signal in the *pils6-1* (*D*) and weaker signal in the *PILS6*^{OE} (*F*) compared with the wild type. Note that in the pseudocolored visualization, red indicates high and blue indicates low intensity (see the color code bar). Confocal images and quantification of DII-VENUS (*E*) show enhanced fluorescence in the *PILS6*^{OE} compared with the wild type. The white dashed boxes represent defined ROIs used to quantify the respective signal intensities. [Scale bars, 50 μm (*A*–*F*).] $n = 9$ (*C*), 6 (*D*), 7 (*E*), and 6 (*F*) roots. $^{**}P = 0.001$–0.01, $^{***}P < 0.001$, Student's *t* test.

(see also the eFP browser bar.utoronto.ca/efp/cgi-bin/efpWeb.cgi). Moreover, HT increases auxin signaling in roots by an unknown mechanism (12–14), which motivated us to investigate whether PILS6 may also play a role in integrating ambient temperature into an auxin-dependent growth program.

To investigate the potential transcriptional control of *PILS6*, we combined the PILS6 promoter sequence with the beta-glucoronidase (*GUS*) and *GFP* fusion (*pPILS6::GUS-GFP*) reporter (18). Notably, the same promoter sequence was used and sufficient to complement the *pils6-1* mutant with PILS6-GFP (*SI Appendix*, Fig. S2*E*). We readily detected *PILS6* expression in cotyledons, hypocotyls, and roots (*SI Appendix*, Fig. S3 *A*–*C*), which agrees with the reported endogenous transcript detection and cell-type specific, microarray-based predictions (16, 19, 28).

To investigate the effect of HT stress, we germinated seedlings either under 21 °C (control) and 29 °C (HT), or under 21 °C and transferred 3-d-old seedlings for an additional 3 d under 29 °C. If not specified otherwise, the latter condition was thereafter used as standard procedure. HT treatment had an intriguing dual effect on *PILS6* gene expression. *PILS6* expression was prominently up-regulated in the root region below the collet (*SI Appendix*, Figs. S3 *D*, *E*, and *G*), but specifically down-regulated in the root apex of seedlings exposed to HT (*SI Appendix*, Fig. S3 *F* and *H*). In agreement with *PILS6* down-regulation in root tips, HT treatment also diminished the PILS6 protein levels in *PILS6::PILS6-GFP*-expressing root meristem (Fig. 3*A*), proposing a potential role of PILS6 in root adaptation to HT.

We next analyzed PILS6-GFP in the root meristem of *PILS6*^{OE} seedlings. Despite its constitutive expression, the PILS6-GFP level in the root meristem was strongly reduced within hours of exposure to HT and remained down-regulated after 3 d of exposure (Fig. 3 *B* and *C* and *SI Appendix*, Fig. S4*A*). Notably, the ER control marker line *35S::HDEL-GFP* (29) was not down-regulated by HT (Fig. 3*C* and *SI Appendix*, Fig. S4 *B* and *C*), suggesting a specific posttranslational impact of HT on PILS6 protein levels. Notably, HT also diminished the PILS6-GFP fluorescence in the differentiated root cells below the collet (*SI Appendix*, Fig. S4*D*) and in cotyledons (*SI Appendix*, Fig. S4*E*). This suggests that HT induces an overall down-regulation of PILS6 proteins and this post-translational mechanism thereby also overrules the transcriptional up-regulation in some tissues.

HT has been shown to increase auxin signaling rates in roots (12, 13), which is consistent with its negative impact on PILS6 proteins. In agreement with these reports, both *pDR5rev::GFP* and *pDR5rev::mRFPer* showed a strong increase in roots when exposed to HT, which was particularly prominent in the quiescent center (QC) and uppermost columella (C) cells (Fig. 3 *D* and *E* and *SI Appendix*, Fig. S4 *F* and *G*). Unfortunately, we could not complement these data with the use of the auxin input marker R2D2, because both the auxin-sensitive D2 as well as its insensitive counterpart R2 were sensitive to HT (*SI Appendix*, Fig. S4*H*).

Next we tested whether PILS6 modulates HT-induced auxin signaling. We detected stronger HT-induced auxin signaling rates in the root tips of *pils6-1* mutant compared with wild-type seedlings (Fig. 3*D* and *SI Appendix*, Fig. S4*F*). The accelerated response of *pils6* mutant to HT indicates that additional molecular components contribute to HT-dependent control of auxin signaling. In agreement, the protein abundance of *35S::PILS1-GFP*, *35S::GFP-PILS2*, and *35S::PILS5-GFP* (16, 18) was also highly sensitive to HT (*SI Appendix*, Fig. S4 *I*–*K*), proposing functional redundancy.

As expected, the relative increase in auxin signaling response was also increased in *PILS6*^{OE} (Fig. 3*E* and *SI Appendix*, Fig. S4*G*), most probably as a consequence of HT-dependent down-regulation of PILS6 protein. Thus, similar to previous observations (12, 13), we confirm that HT affects auxin signaling in roots and, in addition, we reveal that HT-dependent regulation of PILS6 abundance contributes to nuclear auxin signaling rates in roots.

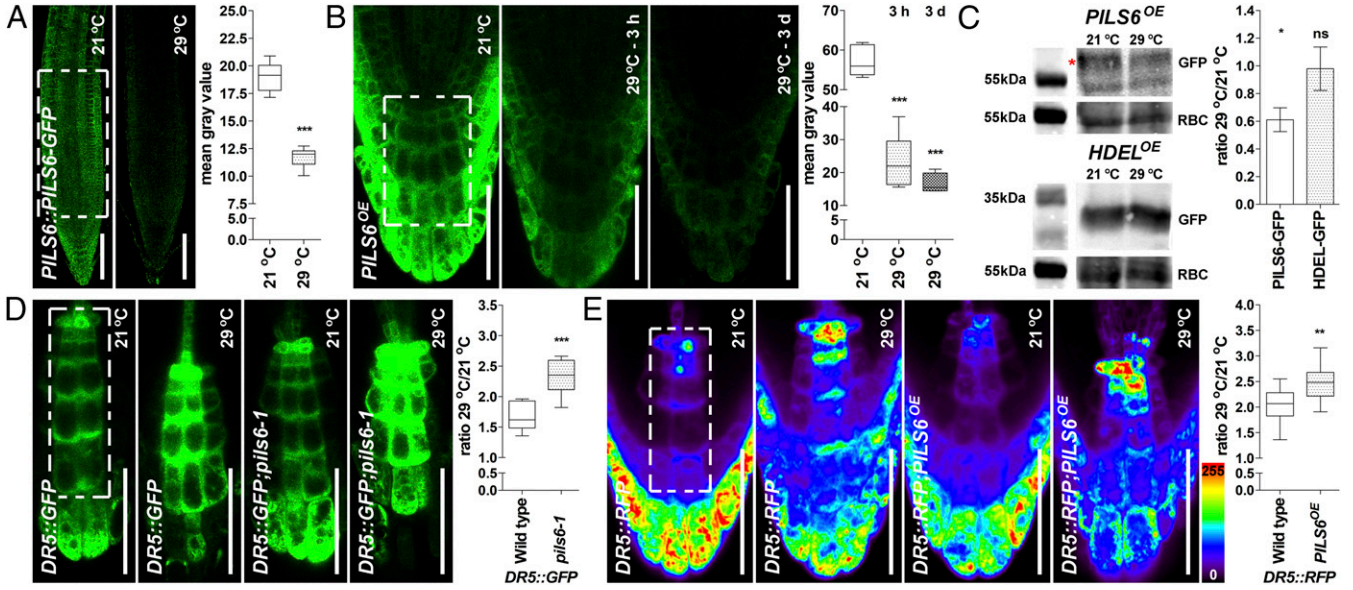

Fig. 3. HT affects PILS6 protein level and PILS6-dependent auxin signaling. (*A*–*C*) HT down-regulates PILS6 protein level. Confocal images and quantification of PILS6-GFP fluorescence show that HT reduces the PILS6 protein levels in roots of *PILS6::PILS6-GFP* (*A*) and *PILS6*^{OE} (*B*). Note that the response of PILS6 protein to HT is fast, showing dramatic reduction (about 60%) already after 3 h. Immunoblot with anti-GFP antibody and quantification of signal intensity (*C*) showing that HT down-regulates protein levels in *PILS6*^{OE} seedlings, but not in *35S::HDEL-GFP* (*HDEL*^{OE}) control line. RuBisCo (RBC) antibody was used for normalization. The red asterisk marks the PILS6-GFP, which runs above a nonspecific band. Please note that the 55kDa molecular weight marker for RBC is duplicated because the loading controls originated from the same protein immunoblot. The statistical evaluation shows the differences between the respective 21 °C and 29 °C values. (*D* and *E*) HT affects PILS6-dependent auxin signaling. Confocal images and quantification of *DR5::GFP* (*D*) or *DR5::RFP* (*E*), showing a relative increase in auxin response in roots of *pils6-1* (*D*) and *PILS6*^{OE} (*E*) when exposed to HT. The white dashed boxes represent defined ROIs in the most representative regions of the root, used to quantify the respective signal intensities. [Scale bars, 100 μm (*A*) and 50 μm (*B*, *D*, and *E*).] $n = 7$ (*A*), 6 (*B*), 9 (*D*), and 12 (*E*) roots. ns, not significant; $*P = 0.01$–0.05, $**P = 0.001$–0.01, $***P < 0.001$, Student's *t* test (*A* and *C*–*E*) or one-way ANOVA (*B*).

Given the importance of PILS6 for nuclear auxin input and consequently root organ growth, we next assessed the contribution of PILS6 to HT-dependent root growth. For this, we germinated seedlings at 21 °C and transferred 4-d-old seedlings for an additional 3 d under 29 °C. As expected, wild-type seedlings showed increased primary root growth when shifted to HT (Fig. 4*A* and *SI Appendix*, Fig. S5*A*). This HT response is presumably linked to a faster transition of meristematic cells into the elongation zone, leading to smaller root meristems (14) (Fig. 4*B*). *pils6* mutant also showed root growth promotion in response to HT (Fig. 4*A* and *SI Appendix*, Fig. S5*A*). Despite some variation in the amplitude of response to HT (*SI Appendix*, Fig. S5*A*), *pils6-1* mutant roots showed a relative reduction in the HT-induced root growth, which also correlated with a stronger impact on root meristem size compared with wild-type seedlings (Fig. 4 *A* and *B* and *SI Appendix*, Fig. S5*A*). In agreement with its negative impact on PILS6 protein levels, HT conditions partially rescued the short root phenotype of *PILS6*^{OE} (Fig. 4*A* and *SI Appendix*, Fig. S5*A*). *PILS6*^{OE} roots remained overall shorter, but showed a relative enhancement of root length, correlating with a more balanced reduction in root meristem size compared with wild type (Fig. 4 *A* and *B* and *SI Appendix*, Fig. S5*A*). These findings suggest a PILS6-dependent role in setting optimal auxin signaling rates for root growth responses to HT. In summary, our data propose that PILS6 controls nuclear abundance of auxin, which is implemented by HT sensing to modulate nuclear auxin responses and subsequently root growth.

Concluding Remarks

Here we show that ER-localized putative auxin carrier PILS6 restricts the nuclear availability and signaling of auxin. This agrees with a presumed role of PILS proteins in transporting auxin into the ER lumen, which limits auxin diffusion into the nucleus and thereby sets the cellular sensitivity to auxin. Besides PILS6, also PILS2, PILS3, and PILS5 have been shown to repress auxin signaling (16–18). Intriguingly, PILS2, -3, -5, and -6 belong to distinct subfamilies (19), which suggests that members of all PILS subfamilies have conserved roles in restricting auxin signaling in *Arabidopsis*. We recently showed that light perception triggers the expression of *PILS2* and *-3*, allowing this environmental cue to induce an auxin signaling minimum and differential growth during apical hook development (18). Here we show that an increase in ambient temperature negatively affects PILS6 abundance, which consequently increases auxin signaling and modulates root growth. Accordingly, we assume that PILS proteins have general importance for integrating environmental cues into growth programs.

PIF4-dependent auxin biosynthesis integrates elevated temperature with increased auxin levels and growth in shoots, but not in roots (14). Hence, the role of auxin in HT-induced root growth remained controversial. Our findings, at least partially, explain the observed increase in auxin signaling (12, 13), which occurs despite the absence of PIF4-induced auxin biosynthesis (14). Accordingly, we conclude that PILS6 is part of an alternative subcellular mechanism, linking HT to increased auxin responses in roots.

Materials and Methods

Plant Material. *A. thaliana* ecotype Columbia 0 was used as the wild type. 35S::PILS1-GFP (PILS1^{OE}), 35S::GFP-PILS2 (PILS2^{OE}), 35S::PILS5-GFP (PILS5^{OE}), 35S::PILS6-GFP (PILS6^{OE}) (16), PILS6::GUS-GFP (18), pDR5rev::GFP (25), pDR5rev::mRFP1er (26), R2D2 (24), DII-VENUS (23), mDII-VENUS (23), CYCB1;1::GUS (21), and 35S::HDEL-GFP (29) have been described previously. pils6-1 (SALK_130335.46.50) and pils6-2 (SALK_074172.15.55) were obtained from Nottingham Arabidopsis Stock Centre (20).

Growth Conditions. To avoid any germination-related issues and their potential effect on the phenotype, all experiments have been performed using fresh seeds. Seeds were sterilized either (*i*) overnight with chlorine gas, followed by a few hours of aeration or (*ii*) 1–2 min with 70% ethanol,

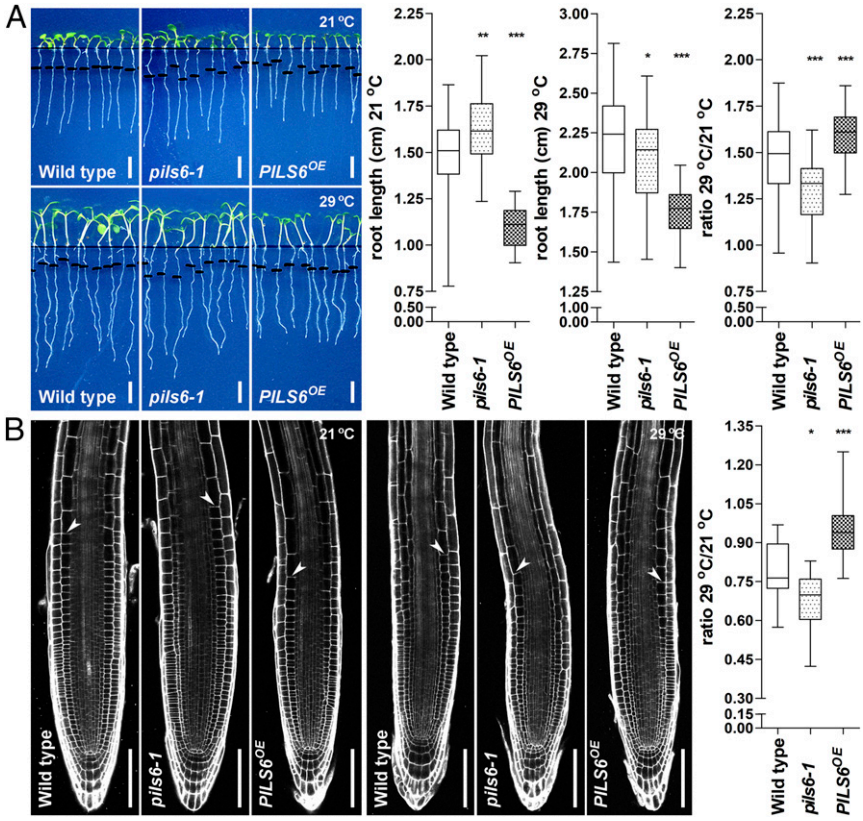

Fig. 4. PILS6 regulates root growth under HT. (*A* and *B*) PILS6 affects root growth under HT. Scanned images, quantification of the root segment grown after 3-d exposure to 21 °C (control) or 29 °C (HT), and calculated ratio showing that *pils6-1* and *PILS6*^{OE} affect root growth under HT compared with the wild type (*A*). Confocal images and (relative) quantification of wild type, *pils6-1*, and *PILS6*^{OE} root meristems exposed for 3 d to 21 °C or 29 °C (*B*). Root meristem is depicted as the distance between the quiescent center and the uppermost first cortical cell that is twice as long as it is wide. [Scale bars, 500 μm (*A*) and 100 μm (*B*).] n = 32–34 roots (*A*) and 20 root meristems (*B*). **P* = 0.01–0.05, ***P* = 0.001–0.01, ****P* < 0.001, one-way ANOVA.

followed by drying. Afterward, seeds were plated on one single line, uniformly spaced, in the upper part of Petri dishes containing 50 mL solidified agar medium, made of 0.8% agar, 0.5× Murashige and Skoog (MS) medium, and 1% sucrose (pH 5.9). Before germination, the seeds were stratified for 3 d in the dark at 4 °C. Then, seedlings were grown on vertically oriented plates under standard growth conditions: plant cabinet equipped with cool-white fluorescent bulbs placed above, and set at about 140 $\mu mol \cdot m^{-2} \cdot s^{-1}$, long day photoperiod, and 21 °C.

For HT-related experiments, two growth cabinets were equipped with overhead LED cultivation lights (Ikea, 703.231.10), at an irradiance of 150 $\mu mol \cdot m^{-2} \cdot s^{-1}$, long day photoperiod, and set at 21 °C (control) or 29 °C (HT treatment). For microscopy, the seedlings were allowed to grow on vertically oriented plates for 6 d under 21 °C (control) or 3 d under 21 °C followed by another 3 d under 29 °C (HT treated). For root length evaluation, the seedlings were allowed to grow on vertically oriented plates for 7 d under 21 °C (control) or 4 d under 21 °C followed by another 3 d under 29 °C (HT treated).

Quantification of Cotyledons, Rosettes, and Root Phenotype. For cotyledons and rosette measurements, seedlings were grown initially on vertically oriented plates for 5 d, then turned to a horizontal position and allowed to grow for 3 (cotyledons) or 7 (rosettes) additional days. For root length measurements, seedlings were grown on vertically oriented plates. For root response to HT, we marked the position of each 4-d-old root tip and measured only the root segment grown after 3 d under 21 °C (control) or 29 °C (HT). Plates were scanned with an Epson Perfection V700 scanner. Rosette area and root length were measured by using ImageJ 1.41 software (https://imagej.nih.gov/ij/).

Quantification of Root Meristem. Root meristems of 6-d-old seedlings grown under 21 °C (control) or 3-d-old seedlings grown under 21 °C followed by 3 d under 29 °C (HT treated) were imaged by a Leica TCS SP5 confocal microscope. Prior to imaging, seedlings were stained with propidium iodide (0.02 mg/mL). The "quantify" tool of Leica software (LAS AF Lite) was used for quantification. We defined the meristem size as the distance between the quiescent center and the uppermost first rectangle cortical cell that is twice as long as it is wide (30).

GUS Staining. GUS staining was performed and quantified as described previously (31). Before staining, seedlings were fixed in 90% cold acetone for 1 h on ice, then washed in phosphate buffer for 1 h at room temperature. Seedlings were stained for 4–5 h (*CYCB1;1::GUS*) or overnight (*pPILS6::GUS-GFP*). To quantify the signal intensity, we defined a region of interest (ROI) capturing the most representative signal distribution. This region is indicated in the figures and was kept constant (size and shape) for all analyzed samples.

Cloning. Cloning was performed as described in Barbez et al. (16). To generate *PILS6::PILS6-GFP*, the full genomic fragment was cloned into the pDONR221 and the 1.2-kb promoter region into the pDONR-P4P1, by using the primers listed in *SI Appendix*, Table S1. These entry clones and the GFP-containing entry clone were subsequently transferred to the Gateway-compatible destination vector pK7m34GW.0 (32). Transformed lines were selected on kanamycin.

qRT-PCR Analysis. We used 7-d-old seedlings and the InnuPREP Plant RNA Kit (Analytic Jena) to extract total RNA according to the manufacturer's recommendation. Prior to cDNA synthesis, the RNA samples were treated with InnuPREP DNase I (Analytic Jena). cDNA was synthesized from 1 μg of RNA using the iSCRIPT cDNA Synthesis Kit from Bio-Rad and according to the manufacturer's recommendation. qRT-PCR was carried out in a C1000 Touch Thermal Cycler equipped with the CFX96 Touch Real-Time PCR Detection System (Bio-Rad), using a Takyon qPCR Kit for SYBER assay (Eurogentec) and according to the manufacturer's recommendation. We used the *PILS6* gene and *ACTIN2* control primers listed in *SI Appendix*, Table S1. *PILS6* gene expression was normalized to the expression of *ACTIN2*.

Western Blot. Six-day-old seedlings (control seedlings were grown for 6 d under 21 °C; HT-treated seedlings were grown for 3 d under 21 °C followed by another 3 d under 29 °C) were ground to fine powder in liquid nitrogen and solubilized with extraction buffer [25 mM Tris, pH 7.5, 10 mM $MgCl_2$, 15 mM EGTA, 75 mM NaCl, 1 mM DTT, 0.1% Tween-20, with freshly added proteinase inhibitor mixture (Roche)]. After spinning down for 30 min at 4 °C with 14,000 rpm, the protein concentration was assessed using the Bradford method. Membranes were probed with a 1:1,000 dilution of GFP antibody (11814460001, Roche). Goat IRDye 800CW anti-mouse (926–32210, LI-COR) was used (1:20,000) as secondary antibody. The signals were detected and quantified using the Odyssey Imagine System (LI-COR). RuBisCo signal was detected in the 700-nm fluorescence channel and used for normalization. Samples were used for three independent technical replicates.

Confocal Imaging and Quantification. Imaging was performed by using a Leica TCS SP5 confocal microscope, equipped with HyD in addition to the standard photomultiplier tubes (PMT). The HyD has been used for detecting *PILS6::PILS6-GFP*. To image DII-VENUS and mDII-VENUS, we used a Leica TCS SP8 equipped with a white laser, allowing the separation of GFP and YFP fluorophores. The fluorescence signal intensity (mean gray value) of the presented markers was quantified by using the quantify tool of the Leica software (LAS AF Lite). For all markers, we defined a ROI in the region that showed the most representative signal distribution without or in response to HT. ROIs are indicated in the figures. We used the same ROI (size and shape) to analyze all images of the respective experiment. Notably, *DR5::GFP* and *DR5::RFP* reporter lines show slight signal deviations in the most mature columella and lateral root cap cells. We hence avoided signal quantification of these regions. For HT-induced changes in DR5 signal intensity, the ROI was restricted to the quiescent center and columella cell types (as depicted in the figures) showing similar signal distributions and response in *DR5::GFP* and *DR5::RFP*.

Data Analysis. We used Excel to organize data and GraphPad Prism 5 software for statistical analysis and graphing. For statistical analysis of the raw data, we used one-way ANOVA and Tukey's multiple comparison test for the experiments with several genotypes (e.g., wild-type control, *pils6* mutants and *PILS6^{OE}*), and Student's *t* test for the experiments with two genotypes/conditions (e.g., fluorescence intensity in two different backgrounds or conditions).

The most representative images are shown throughout the article. The experiments have been performed in triplicates or more.

ACKNOWLEDGMENTS. We thank J. Friml, A. Maizel, T. Vernoux, and D. Weijers for providing the published marker lines; M. Debreczeny for imaging expertise; L. Mach and R. Strasser for sharing equipment; and the BOKU-Vienna Institute of BioTechnology (VIBT) Imaging Center for access. This work was supported by the Vienna Science and Technology Fund (J.K.-V.), the Austrian Science Fund (FWF) (Projects: P26568-B16 and P26591-B16 to J.K.-V.), the European Research Council (AuxinER–ERC Starting Grant to J.K.-V.), the European Molecular Biology Organization (ALTF 795-2012 to E.F.), FWF-Hertha Firnberg (T728-B16 to E.F.), and FWF-Elise Richter (V690-B25 to E.F.).

1. Rivero L, et al. (2014) Handling Arabidopsis plants: Growth, preservation of seeds, transformation, and genetic crosses. *Methods Mol Biol* 1062:3–25.
2. Liu J, Feng L, Li J, He Z (2015) Genetic and epigenetic control of plant heat responses. *Front Plant Sci* 6:267.
3. Davies PJ (2010) *The Plant Hormones: Their Nature, Occurrence, and Functions. Plant Hormones* (Springer, Dordrecht), pp 1–15.
4. Shibasaki K, Rahman A (2013) Auxin and temperature stress: Molecular and cellular perspectives. *Polar Auxin Transport*, eds Chen R, Baluška F (Springer, Berlin), pp 295–310.
5. Ahammed GJ, Li X, Zhou J, Zhou Y-H, Yu J-Q (2016) Role of hormones in plant adaptation to heat stress. *Plant Hormones Under Challenging Environmental Factors*, eds Ahammed GJ, Yu J-Q (Springer Netherlands, Dordrecht), pp 1–21.
6. Jung JH, et al. (2016) Phytochromes function as thermosensors in Arabidopsis. *Science* 354:886–889.
7. Legris M, et al. (2016) Phytochrome B integrates light and temperature signals in Arabidopsis. *Science* 354:897–900.
8. Gray WM, Ostin A, Sandberg G, Romano CP, Estelle M (1998) High temperature promotes auxin-mediated hypocotyl elongation in Arabidopsis. *Proc Natl Acad Sci USA* 95:7197–7202.
9. Koini MA, et al. (2009) High temperature-mediated adaptations in plant architecture require the bHLH transcription factor PIF4. *Curr Biol* 19:408–413.
10. Franklin KA, et al. (2011) Phytochrome-interacting factor 4 (PIF4) regulates auxin biosynthesis at high temperature. *Proc Natl Acad Sci USA* 108:20231–20235.
11. Sun J, Qi L, Li Y, Chu J, Li C (2012) PIF4-mediated activation of YUCCA8 expression integrates temperature into the auxin pathway in regulating arabidopsis hypocotyl growth. *PLoS Genet* 8:e1002594.
12. Hanzawa T, et al. (2013) Cellular auxin homeostasis under high temperature is regulated through a sorting NEXIN1-dependent endosomal trafficking pathway. *Plant Cell* 25:3424–3433.
13. Wang R, et al. (2016) HSP90 regulates temperature-dependent seedling growth in Arabidopsis by stabilizing the auxin co-receptor F-box protein TIR1. *Nat Commun* 7:10269.
14. Martins S, et al. (2017) Brassinosteroid signaling-dependent root responses to prolonged elevated ambient temperature. *Nat Commun* 8:309.
15. Fei Q, Wei S, Zhou Z, Gao H, Li X (2017) Adaptation of root growth to increased ambient temperature requires auxin and ethylene coordination in Arabidopsis. *Plant Cell Rep* 36:1507–1518.
16. Barbez E, et al. (2012) A novel putative auxin carrier family regulates intracellular auxin homeostasis in plants. *Nature* 485:119–122.
17. Barbez E, et al. (2013) Single-cell-based system to monitor carrier driven cellular auxin homeostasis. *BMC Plant Biol* 13:20.
18. Béziat C, Barbez E, Feraru MI, Lucyshyn D, Kleine-Vehn J (2017) Light triggers PILS-dependent reduction in nuclear auxin signalling for growth transition. *Nat Plants* 3:17105.
19. Feraru E, Vosolsobě S, Feraru MI, Petrášek J, Kleine-Vehn J (2012) Evolution and structural diversification of PILS putative auxin carriers in plants. *Front Plant Sci* 3:227.
20. Alonso JM, et al. (2003) Genome-wide insertional mutagenesis of Arabidopsis thaliana. *Science* 301:653–657.
21. Colón-Carmona A, You R, Haimovitch-Gal T, Doerner P (1999) Technical advance: Spatio-temporal analysis of mitotic activity with a labile cyclin-GUS fusion protein. *Plant J* 20:503–508.
22. Barbez E, Kleine-Vehn J (2013) Divide Et impera–Cellular auxin compartmentalization. *Curr Opin Plant Biol* 16:78–84.
23. Brunoud G, et al. (2012) A novel sensor to map auxin response and distribution at high spatio-temporal resolution. *Nature* 482:103–106.
24. Liao CY, et al. (2015) Reporters for sensitive and quantitative measurement of auxin response. *Nat Methods* 12:207–210, 202 p following 210.
25. Benková E, et al. (2003) Local, efflux-dependent auxin gradients as a common module for plant organ formation. *Cell* 115:591–602.
26. Marin E, et al. (2010) miR390, Arabidopsis TAS3 tasiRNAs, and their auxin response factor targets define an autoregulatory network quantitatively regulating lateral root growth. *Plant Cell* 22:1104–1117.
27. Kilian J, et al. (2007) The AtGenExpress global stress expression data set: Protocols, evaluation and model data analysis of UV-B light, drought and cold stress responses. *Plant J* 50:347–363.
28. Brady SM, et al. (2007) A high-resolution root spatiotemporal map reveals dominant expression patterns. *Science* 318:801–806.
29. Brandizzi F, et al. (2003) ER quality control can lead to retrograde transport from the ER lumen to the cytosol and the nucleoplasm in plants. *Plant J* 34:269–281.
30. Löfke C, Dünser K, Scheuring D, Kleine-Vehn J (2015) Auxin regulates SNARE-dependent vacuolar morphology restricting cell size. *eLife,* 4.
31. Béziat C, Kleine-Vehn J, Feraru E (2017) Histochemical staining of β-Glucuronidase and its spatial quantification. *Methods Mol Biol* 1497:73–80.
32. Karimi M, Inzé D, Depicker A (2002) GATEWAY vectors for Agrobacterium-mediated plant transformation. *Trends Plant Sci* 7:193–195.